NURETH14-273

CFD APPLICATION TO PWR SUBCHANNEL VOID DISTRIBUTION BENCHMARK

W. K. In¹, C. H. Shin¹ and T. H. Chun¹

¹ Korea Atomic Energy Research Institute, Daejeon, Rep. of Korea

Abstract

A CFD study is performed to simulate the steady-state void distribution benchmark based on the NUPEC PWR Subchannel and Bundle Tests (PSBT). The CFD calculation predicted the void distributions in central typical and thimble subchannels, side subchannel and corner subchannel. The CFD prediction shows a higher void fraction near the heated wall and a migration of void in the subchannel gap region. A measured image of void distribution indicated a locally higher void fraction near the heated wall. The CFD predictions of void fraction and fluid density agree well with the measured ones for the low void test condition. However, the CFD calculations tend to underpredict the void fraction and overpredict the fluid density as the void fraction increases.

1. Introduction

A subcooled boiling flow in a rod bundle is an important phenomenon in a nuclear reactor system. Most nuclear fuel elements loaded in the reactor generally consist of rod bundles with the coolant flowing axially through the subchannels formed between the rods. The fuel rods are arranged in either square or equilateral triangular pitched arrays. Subcooled boiling may be encountered in nuclear reactors under certain conditions. An understanding of the three-dimensional distributions of the flow and phases in rod bundles, used especially as nuclear fuel elements, is of major interest to the nuclear power industry for their safe and reliable operation. Recently, there have been some studies using computational fluid dynamics (CFD) in the multi-dimensional analysis of multiphase flow problems. The application of CFD to multiphase flows still requires extensive validation of the computational technique and the closure models as outlined by Yadigaroglu *et al.* [1].

There have been some numerical studies on high-pressure and low-pressure subcooled boiling flows in a simple geometry. Kurul [2] formulated a multidimensional two-fluid model and applied this model to various subcooled boiling phenomena in a heated channel. He also proposed heat transfer modes at a wall and presented a mechanistic model for wall heat transfer during a forced-convection flow. Anglart [3] applied a multidimensional two-fluid model to a high-pressure (4.5 MPa) boiling bubbly flow in vertical tubes and showed a good agreement between the predictions and measurements of the temperature and void distribution. Anglart and Nylund [4] implemented a two-fluid model into a commercial CFD code and predicted the void distribution in a circular channel with a single heated rod and circular channels with six heated rods with a system pressure of approximately 5 MPa. They predicted void fraction distributions in the subcooled and bulk boiling regions that show a satisfactory agreement with the measurements. Yeoh and Tu [5] employed a three-dimensional two-fluid model coupled with

population balance equations to predict a subcooled boiling flow at a low pressure in a vertical annular channel with the influence of bubble coalescence and break-up. Using the boiling model implemented in the CFD code CFX-4, Krepper *et al.* [6] simulated boiling experiments in a heated tube and a channel around a heated rod. The comparisons with the experiments showed a good agreement for the pressures at about 1.5 to 5 MPa but a significant underestimation of the volume fraction for the lower pressures. He also pointed out that the largest influences are found for the bubble departure diameter and for the mean bubble diameter. In and Chun [7] performed a CFD simulation of a BWR fuel bundle test for void distribution benchmark. This CFD analysis reproduced an overall radial void distribution trend which was less vaporous in the central part of the bundle and more vaporous in the periphery. However, the comparison of detailed in-channel void distributions shows a somewhat large discrepancy between the CFD and experimental results.

OECD/NRC established the international PSBT benchmark based on the NUPEC database to encourage the development of novel mechanistic computational approaches applicable to the multi-phase flow phenomena inside fuel bundles. The void distribution benchmark provides measured void fraction data over a wide range of geometrical and operating conditions in single subchannel and fuel bundle. This CFD study simulated the boiling flow in four different types of the single subchannel, i.e., typical center, thimble center, side and corner cells. The single subchannel test section is uniformly heated over 1555 mm by direct heating method. The CFD code, ANSYS CFX-12.1 [8] was used to predict the void distribution inside the single subchannel.

2. Multiphase flow model

The multiphase flow model used in this CFD analysis is the two-fluid model in which liquid(water) and vapour(steam) are considered as continuous and dispersed fluids, respectively. The two-fluid model uses the interfacial area per unit volume between the phases to model interfacial transfer of momentum, heat and mass. The interfacial momentum transfer rates included in this CFD simulation are drag force, lift force, wall lubrication force and turbulent dispersion force. Heat transfer across a phase boundary is predicted using an inter-phase heat transfer coefficient and an interfacial area. The inter-phase mass transfer is calculated depending on the liquid temperature, i.e., a bulk condensation or evaporation. A wall boiling model is also employed to simulate the bubble generation on a heated wall surface. The wall heat is assumed to be partitioned into three parts, i.e., convective, quenching and evaporative heat transfers.

2.1 Governing equations for multiphase

The hydrodynamic conservation equations of mass, momentum and energy for each phase can be written as:

$$\frac{\partial}{\partial t} (\alpha_k \rho_k) + \nabla \cdot (\alpha_k \rho_k U_k) = \sum_{j=1, j \neq k}^{N_p} (\Gamma_{kj} - \Gamma_{jk})$$
(1)

The 14th International Topical Meeting on Nuclear Reactor Thermalhydraulics, NURETH-14 Toronto, Ontario, Canada, September 25-30, 2011

$$\frac{\partial}{\partial t} (\alpha_k \rho_k U_k) + \nabla \cdot (\alpha_k \rho_k U_k U_k) = \nabla \cdot \left[\alpha_k \mu_k^e \left(\nabla U_k + (\nabla U_k)^T \right) \right] - \alpha_k \nabla p_k + \alpha_k \rho_k g$$

$$+ \sum_{i=1,i\neq k}^{N_p} \left(\Gamma_{kj} U_j - \Gamma_{jk} U_k \right) + \sum_{i=1,i\neq k}^{N_p} M_{kj}$$
(2)

$$\frac{\partial}{\partial t} (\alpha_k \rho_k H_k) + \nabla \cdot (\alpha_k \rho_k U_k H_k - \alpha_k \lambda_k^e \nabla T_k) = \frac{\partial}{\partial t} (\alpha_k p_k) + E_k + \sum_{j=1, j \neq k}^{N_p} (\Gamma_{kj} H_j - \Gamma_{jk} H_k) + \sum_{j=1, j \neq k}^{N_p} Q_{kj}$$
(3)

Here, α_k, p_k, U_k, T_k and H_k are the volume fraction, pressure, velocity, temperature and enthalpy of phase k, respectively and N_p is the number of phases. Γ_{kj} , M_{kj} and Q_{kj} are the inter-phase transfer of the mass, momentum and energy from phase j to phase k, and μ_k^e and λ_k^e are the effective viscosity and thermal conductivity of phase k, respectively. Additional variables are the gravitational acceleration, g and the heat source to phase k, E_k .

2.2 Closure models

The multiphase flow model based on the conservation equations (1)-(3) requires constitutive equations to achieve the closure. The accuracy of the multiphase flow model largely depends on how one models the constitutive terms including the phase interaction terms (Γ_{ki} , M_{ki} and Q_{ki}).

Since the present CFD analysis is to simulate the vapour-liquid two-phase flow, the closure relationships for the interaction terms between a continuous liquid phase and a dispersed vapour phase are required. The closure models are derived for the transport of the momentum, energy, and mass of each phase across the interfaces. A closure model for the two-phase turbulence is also required.

The interphase momentum transfer in eq. (2) indicates the rate of the momentum transfer per unit volume at the interface which is expressed as a superposition of the terms representing different physical mechanisms. The individual interfacial forces are the drag force, virtual mass force, lift force, lubrication force and the turbulent dispersion force, respectively.

$$M_{lg} = M_{lg}^d + M_{lg}^{vm} + M_{lg}^L + M_{lg}^{LW} + M_{lg}^{TD}$$
(4)

The total drag force per unit volume on the liquid or on the vapour can be expressed as (Ishii and Mishima [9]),

$$M_{lg}^{d} = -M_{gl}^{d} = \frac{3}{4} \frac{C_{D}}{d_{b}} \alpha_{g} \rho_{l} |U_{g} - U_{l}| (U_{g} - U_{l})$$
(5)

Here, C_D and d_b are the drag force coefficient and the mean vapour bubble diameter, respectively. The drag coefficient is obtained from the correlation for the viscous flow region and its modification for a high spherical particle (bubble) concentration (Ishii and Zuber [10]), i.e.,

The 14th International Topical Meeting on Nuclear Reactor Thermalhydraulics, NURETH-14 Toronto, Ontario, Canada, September 25-30, 2011

$$C_D = \frac{24}{\text{Re}_m} \left(1 + 0.15 \,\text{Re}_m^{0.687} \right) \tag{6}$$

$$\operatorname{Re}_{m} = \frac{\rho_{l} \left| U_{g} - U_{l} \right| d_{b}}{\mu_{m}} \tag{7}$$

Here, μ_m is a mixture viscosity. The virtual mass force is neglected in this study because the virtual mass force is insignificant for the lateral phase distribution.

The lift force can be written as (Zun [11]),

$$M_{lg}^{L} = -M_{gl}^{L} = C_{L}\alpha_{g}\rho_{l}\left(U_{g} - U_{l}\right) \times \left(\nabla \times U_{l}\right)$$
(8)

Here, C_L is the lift force coefficient which was set to 0.06 [6]. This force due to the "shear" lift is perpendicular to the rotation vector and the bubble's velocity vector. Recently, Tomiyama *et al.* [12] and Hibiki and Ishii [13] evaluated the net lift coefficient, i.e., the sum of shear- and wake-induced lift coefficient and proposed a correlation yielding the bubble diameter dependency. They showed that the net lift coefficient changes its sign from positive to negative for large bubbles.

The term M_{lg}^{LW} represents the wall lubrication force that is in the normal direction away from a wall and decays with the distance from the wall. This is a force to account for the change of the lift force near a wall due to the change of the velocity distribution around the vapour bubble. The force is given by (Antal *et al.*, [14])

$$M_{lg}^{LW} = -M_{gl}^{LW} = \frac{\alpha_g \rho_l \left(U_g - U_l \right)^2}{d_b} \cdot Max \left(C_{wl} + C_{w2} \frac{d_b}{y_w}, 0 \right) n_w$$
 (9)

where y_w is the distance from the wall and n_w is the normal to the wall. The coefficients C_{w1} and C_{w2} were set to -0.025 and 0.075 [6], respectively. This means the force only exists in a region of less than 5 bubble diameters from the wall.

The last term in eq. (4) represents the effect of the dispersion of the bubbles in a turbulent liquid flow. This force depends on the amount of turbulence in the continuous phase and the gradient of the volume fraction. Burns *et al.* [15] derived the turbulent dispersion force based on the Favre averaged drag model as:

$$M_{lg}^{TD} = -M_{gl}^{TD} = C_{TD}C_{d,lg}\frac{v_l^t}{\sigma_\alpha} \left(\frac{\nabla \alpha_g}{\alpha_g} - \frac{\nabla \alpha_l}{\alpha_l}\right)$$
(10)

where C_{TD} , v'_l and σ_{α} are the turbulent dispersion coefficient, kinematic eddy viscosity and volume fraction turbulent Prandtl number, respectively. The turbulent dispersion coefficient

 (C_{TD}) and turbulent Prandtl number (σ_{α}) were assumed to be 1.0 and 0.9, respectively. $C_{d,lg}$ is the resistance coefficient used to define the interphase drag model which can be expressed as:

$$C_{d,lg} = \frac{3}{4} \frac{C_D}{d_h} \alpha_g \rho_l \left| U_g - U_l \right| \tag{11}$$

Heat transfer across a phase boundary with interphase mass transfer is handled by a two resistance model which considers separate heat transfer processes on either side of the phase interface. The two resistance model uses two heat transfer coefficients defined on each side of the phase interface. The fluid–specific heat transfer coefficient is expressed in terms of a non-dimensional Nusselt number:

$$Nu_k = \frac{h_k d_{lg}}{\lambda_k} \tag{12}$$

where λ_k is the thermal conductivity of the phase k and d_{lg} is a characteristic length scale, i.e., bubble diameter for a particle (bubble) in an incompressible fluid. The Nusselt number uses the well-known Ranz-Marshall correlation for the liquid side and is set to infinity for the vapour side. The infinite gas heat transfer coefficient (a zero resistance condition on the vapour side) is to force the interfacial temperature to be the same as the vapour temperature. The Ranz-Marshall correlation is expressed as:

$$Nu_1 = 2 + 0.6 \,\mathrm{Re}^{1/2} \,\mathrm{Pr}^{1/3} \tag{13}$$

The mean bubble diameter is calculated locally as a linear function of liquid subcooling as Anglart and Nylund [4] proposed, i.e.,

$$d_b = \frac{d_{b1} \left(T_{sub} - T_{sub,2} \right) + d_{b2} \left(T_{sub,1} - T_{sub} \right)}{T_{sub,1} - T_{sub,2}}$$
(14)

Here, $d_{b1} = 0.1mm$, $T_{sub1} = 13.5K$, $d_{b2} = 2mm$, $T_{sub2} = -5K$.

The interphase mass transfer in a boiling flow includes the evaporation at the wall and a bulk condensation or evaporation. The mass transfer from a liquid to a vapour at the wall due to an evaporation is neglected in this CFD analysis. In the interior of the flow, the mass transfer rate between the two phases depends on the liquid temperature. When the liquid is subcooled, there is a bulk condensation from the vapour phase to the liquid. When the liquid is superheated, there is a bulk evaporation from the liquid to the vapour. Both of these rates depend on the heat transfer rate and the latent heat (h_{lg})

$$\Gamma_{lg} = \max\left(\frac{h_l A_{lg} \left(T_{sat} - T_l\right)}{h_{lg}}, 0\right) \text{ for } T_l < T_{sat}$$
(15)

The 14th International Topical Meeting on Nuclear Reactor Thermalhydraulics, NURETH-14 Toronto, Ontario, Canada, September 25-30, 2011

$$\Gamma_{gl} = \max\left(\frac{h_g A_{lg} \left(T_l - T_{sat}\right)}{h_{lg}}, 0\right), \text{ for } T_l > T_{sat}$$
(16)

For a flow of spherical bubbles of diameter d_b in a liquid, the interfacial area density can be determined as:

$$A_{lg} = \frac{6\alpha_g}{d_h} \tag{17}$$

The assumption for modeling the two-phase bubbly flow turbulence in the liquid phase is that the shear-induced turbulence and the bubble-induced turbulence can be superposed linearly. Hence, the turbulent viscosity of the liquid phase can be expressed as:

$$\mu_{I}^{t} = \mu_{I}^{t(SI)} + \mu_{I}^{t(BI)} \tag{18}$$

The shear-induced turbulent viscosity is determined from the standard $k - \varepsilon$ model and the bubble-induced turbulent viscosity is expressed as (Sato *et al.*, [16]):

$$\mu_l^{t(SI)} = \rho_l C_\mu \frac{k_l^2}{\varepsilon_l} \tag{19}$$

$$\mu_l^{t(BI)} = \rho_l C_{tb} \frac{d_b}{2} \alpha_g \left| U_g - U_l \right| \tag{20}$$

with the coefficients $C_u = 0.09$ and $C_{tb} = 1.2$.

2.3 Wall boiling model

The wall boiling model used in this study was the wall heat partition model (Kurul [2]) in which the total wall heat flux (Q_w) is split into three parts (Fig. 1). These are the heat transfer rates due to a convection Q_f , due to a quenching Q_q and to an evaporation Q_e , i.e.,

$$Q_w = Q_f + Q_e + Q_q \tag{21}$$

The convective heat transfer rate is given in terms of a local Stanton number for a turbulent convection by:

$$Q_f = St \rho_l C_{pl} U_l (T_w - T_l) A_f \tag{22}$$

Here, T_w is the wall temperature and T_l and U_l are the liquid temperature and velocity in the cell next to the wall. A_f is the fraction of the wall area subjected to a cooling by a convection.

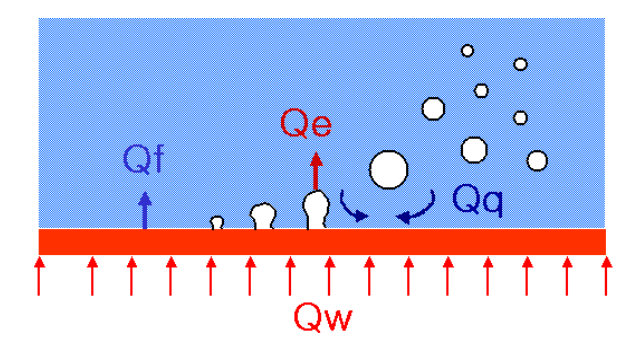


Figure 1 Schematic of wall boiling model.

The heat transfer due to a quenching is expected to occur when fresh liquid comes into contact with a heating surface after a bubble departs. This liquid is assumed to be heated by a transient conduction with a step change in the temperature at the surface. The corresponding heat transfer rate Q_q can be calculated by the relationship (Mikic and Rohsenow [17]):

$$Q_{q} = \frac{2}{\sqrt{\pi}} f \sqrt{t_{w} \lambda_{l} \rho_{l} C_{pl}} \left(T_{w} - T_{l} \right) A_{q}$$
(23)

The heat flux due to a vapor generation at a heating surface can be expressed as

$$Q_e = nf\left(\frac{\pi}{6}d_{bw}^3\right)\rho_g h_{lg}. \tag{24}$$

The parameters used in Eqs. (23) and (24) are the nucleation site density (n), the bubble detachment frequency (f), the bubble departure diameter (d_{bw}) , the waiting time (t_w) and the fraction of the wall area subjected to a cooling by a quenching (A_q) . These parameters are given by the following correlations:

$$n = \left[185\left(T_w - T_{sat}\right)\right]^{1.805} \tag{25}$$

$$f = \sqrt{\frac{4}{3} \frac{g\left(\rho_l - \rho_g\right)}{d_{bw} \rho_l}} \quad t_w = \frac{0.8}{f}$$
 (26)

$$d_{bw} = \min\left[0.0006 \exp\left(-\frac{T_{sat} - T_l}{45}\right), 0.0014\right]$$
 (27)

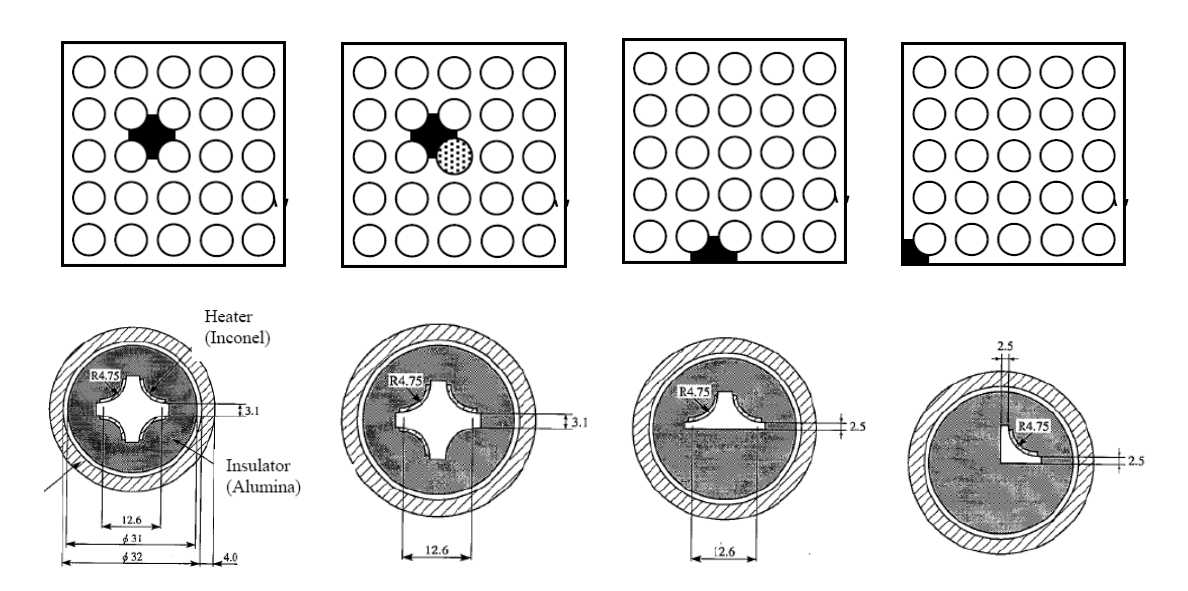
$$A_{q} = \min\left(\pi d_{bw}^{2} n, 1\right) \quad A_{f} = 1 - A_{q}$$
 (28)

3. CFD analysis of PWR subchannel void distribution

This CFD study was performed to simulate the single subchannel void distribution measurements for the OECD/NRC benchmark based on NUPEC PSBT [18]. The single subchannel test section is uniformly heated over 1555 mm by direct heating method. The void measurement was made at 1400 mm from the bottom of the heated section. Figure 2 shows the test sections for the central typical, thimble, side and corner subchannel. This CFD analysis analyzed the boiling flow in four different types of the single subchannel. Table 1 lists the PSBT test conditions simulated in this CFD analysis. The eight (8) test cases were selected depending on the subchannel type and the test conditions. The inlet subcooling decreased from 64 °C to 24 °C for the typical subchannel (S1) and 17 °C to 12 °C for the thimble subchannel (S2). The inlet subcoolings are 30 °C and 26 °C for the side and corner subchannel.

Using a symmetry of test section and flow, only the quadrant of the central(typical) subchannel and the half of the side subchannel were modeled in this CFD analysis. Multi-blocks were employed to model the computational domain with a hexahedral mesh. Total number of mesh is 87360 cells for the quadrant subchannel. Uniform flow and constant temperature were assumed at the inlet boundary and a constant pressure was applied at the outlet boundary. Uniform heat flux and no-slip conditions were used at the heated wall.

Iterative calculations were performed to obtain a converged solution with a false time step and a high resolution differencing scheme (blending of first and second-order upwind schemes). The numerical iteration was continued until both the root-mean-square (RMS) residuals of the governing equations and the variation of flow properties monitored at specified locations were insignificant. In addition, the velocity and volume fraction of liquid and vapor monitored at the outlet boundary were converged to their steady-state values.



Typical subchannel(S1) Thimble subchannel(S2) Side subchannel(S3) Corner subchannel(S4)

Figure 2 Cross sectional view of subchannel test assembly.

Table	1	PSRT	Test	Conditions
- инне				

Run No.	Subchannel	Pressure	Mass flux	Power	Inlet temperature
	type	(kg/cm²a)	$(10^6 \text{ kg/m}^2 \text{hr})$	(kW)	(°C)
1.1222	Typical(S1)	169	11	50	334.7
1.2221	Typical(S1)	150	11	69.8	299.4
1.2223	Typical(S1)	150	11	69.8	319.6
1.2423	Typical(S1)	150	4.9	59.9	299.3
2.1231	Thimble(S2)	169	11	37.5	335.0
2.1232	Thimble(S2)	169	11	37.5	340.0
3.2232	Side(S3)	150	11	30	314.5
4.2253	Corner(S4)	150	11	15	318.0

4. Results and discussion

The eight test conditions in Table 1 were simulated in this CFD study and their CFD results were compared with the measured ones. Figure 3 compares the CFD predictions of void fraction in the subchannel with the CT images for the three cases of Run No. 1.1222, 1.2223 and 2.1232. The predicted void contours show less vapour in the core region and high vapour in the gap region and the near-wall region, which agrees well with the CT measurements. It should be noted in the CT image that the vapour seems to move significantly into the gap region for the high void condition (Run No. 1.2223). However, the CFD prediction shows the high void fraction near the heated rod wall.

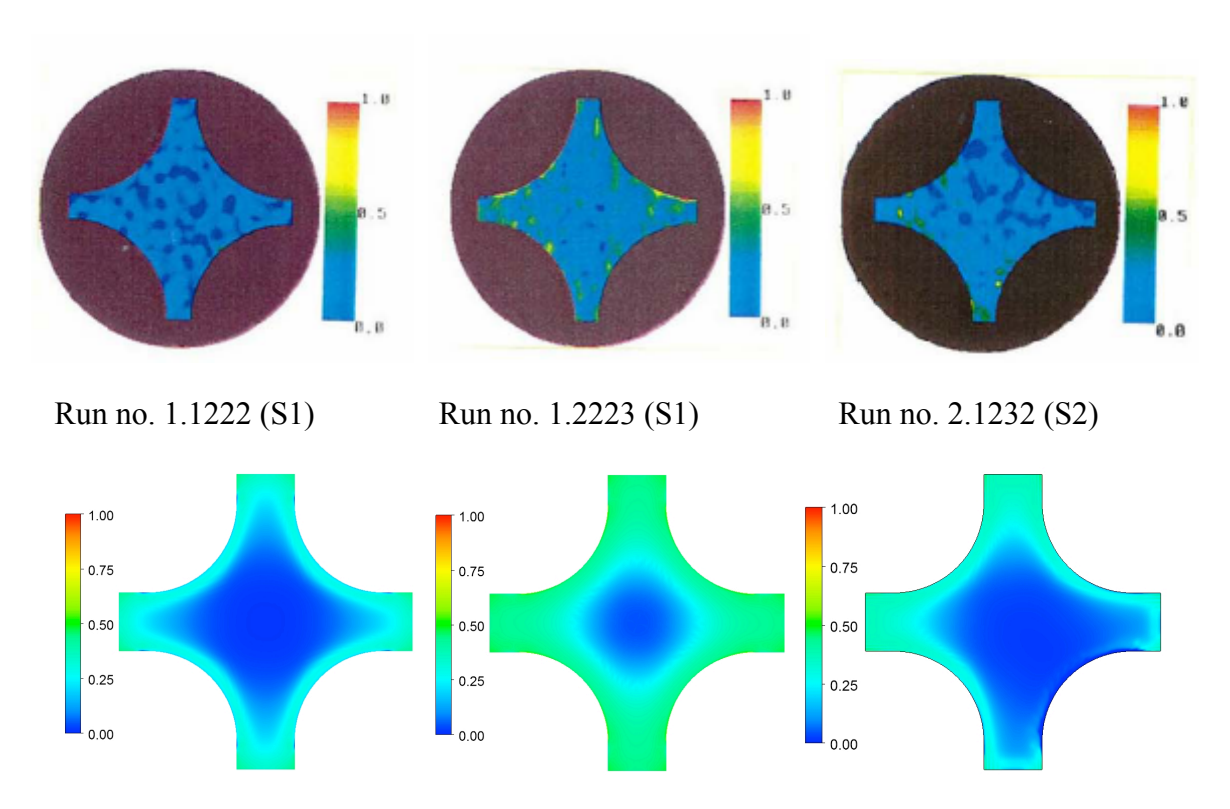


Figure 3 Void fraction contour in the subchannel: (upper) CT image, (low) CFD.

Table 2 lists the subchannel averaged fluid density and void fraction at a measurement plane (1.4 m from the bottom of test section). The CFD predictions agree well with the measured ones for the low void test condition (Run No. 1.1222, 2.1231 & 4.2253). However, the CFD calculations tend to underpredict the void fraction and overpredict the fluid density as the void fraction increases. For the high void conditions (Run No. 1.2423), the CFD predictions show the void fraction as low as 4% and the fluid density as high as 6%. Figure 4 shows the CFD prediction errors for the void fraction and fluid density. It can be seen that the CFD predictions agree with the experimental data within 5% for the void fraction and 10% for the fluid density, respectively.

Table 2 Subchannel Averaged Void Fraction and Fluid Density

Run No.	Fluid dens	ity(kg/m³)	Void fraction		
	PSBT	CFD	PSBT	CFD	
1.1222	517	527	0.142	0.163	
1.2221	621	597	0.048	0.096	
1.2223	456	466	0.311	0.326	
1.2423	357	380	0.508	0.464	
2.1231	550	558	0.096	0.107	
2.1232	501	527	0.181	0.159	
3.2232	553	593	0.132	0.149	
4.2253	554	599	0.087	0.091	

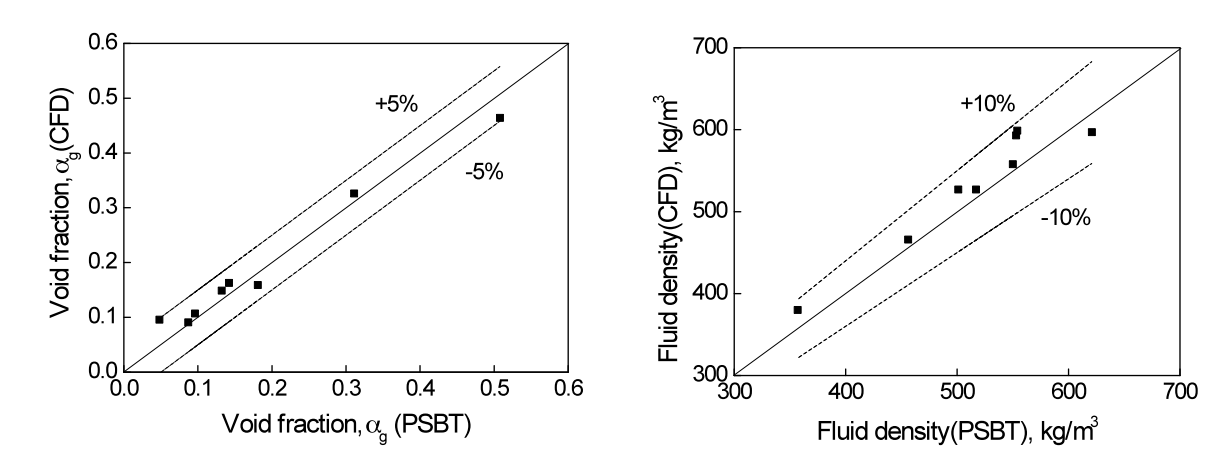


Figure 4 Comparisons of void fraction and fluid density in the subchannel.

The effects of non-drag forces and turbulence model are shown in Fig. 5 for the test run 1.1222. The non-drag forces show a strong influence for the radial void distribution near the rod wall. The lift force and turbulent dispersion force(TD) appear to push the vapour bubble into the wall boundary while the wall lubrication force(LW) directs the bubble to the core region. The void fraction without the LW shows a peak at the wall. The SSG Reynolds stress model predicted higher void fraction in the core region as well as in the near-wall region. This is because the secondary flow predicted by the Reynolds stress model moves the bubble in lateral direction.

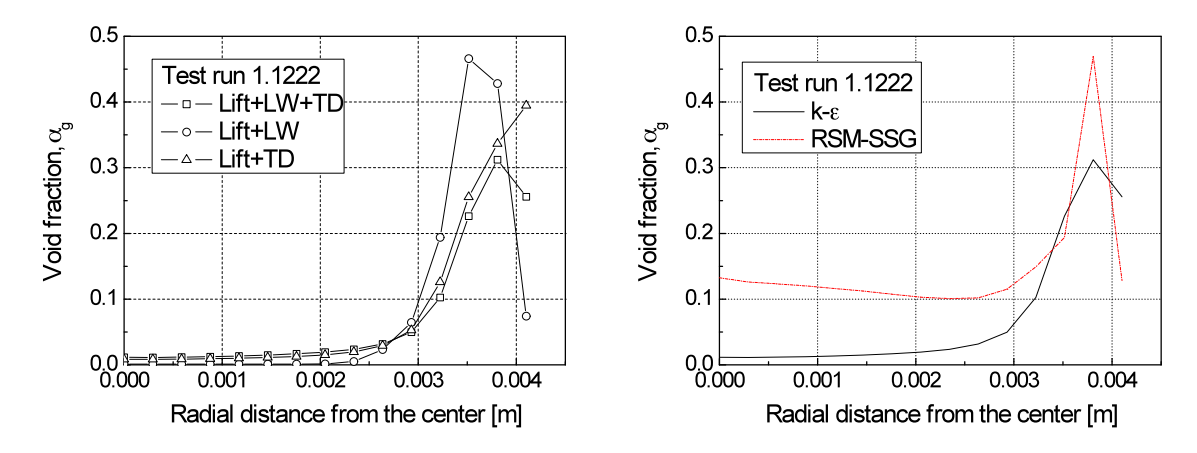


Figure 5 Effects of Non-drag forces and turbulence model.

5. Conclusion

A CFD analysis was performed to simulate the subcooled boiling flow in a single subchannel of a PWR fuel bundle. A two-fluid model and a wall boiling model were used to predict the fluid density as well as the void distribution in four different subchannels. The CFD predictions of the fluid density and void fraction were compared with the measurements. The CFD predictions for the single subchannel agree well with the measured ones for the low void test condition. However, the CFD calculations tend to underpredict the void fraction and overpredict the fluid density as the void fraction increases. The predicted void distribution in the subchannel shows less vapour in the core region and high vapour in the gap region and the near-wall region, which agrees well with the measurements. The CFD predictions for the single subchannel benchmark agree with the experimental data within 5% for the void fraction and 10% for the fluid density. The three-dimensional void distribution predicted in the subchannel should be compared with the fine measurements to further verify the applicability of the CFD method in the future.

Acknowledgments

The authors express their appreciation to the Ministry of Education, Science and Technology (MEST) of Korea for financial support. The authors are very grateful to the OECD NUPEC PSBT Benchmark Program, through which the valuable experiment data for the CFD model assessment was obtained.

6. References

- [1] Yadigaroglu, G., Andreani, M., Dreier, J. and Coddington, P., "Trends and Needs in Experimentation and Numerical Simulation of LWR Safety", Nuclear Engineering and Design, Vol. 221, 2003, pp.205-223.
- [2] Kurul, N., Multidimensional Effects in Two-Phase Flow including Phase Change, Ph. D. Thesis, 1990, Rensselaer Polytechnic Institute.
- [3] Anglart, H., Modeling of Vapor Generation Rate at Wall in Subcooled Boiling Two-Phase Flow, First CFDS International User Conference, Oxford, UK, 1993, pp.183-207.

- [4] Anglart, H. and Nylund, O., "CFDS Application to Prediction of Void Distribution in Two-Phase Bubbly Flows in Rod Bundles," Nuclear Science and Engineering, Vol. 163, 1996, pp.81-99.
- [5] Yeoh, G. H. and Tu, J. Y., "Numerical Simulation of Subcooled Boiling Flow in an Annular Channel with the Influence of Bubble Coalescence and Break-up", *The 10th International Topical Meeting on Nuclear Reactor Thermal Hydraulics(NURETH-10)*, Seoul, Korea, 2003, October 5-9.
- [6] Krepper, E., Koncar, B. and Egorov, Y., "CFD Modeling of Subcooled Boiling Concept, Validation and Application to Fuel Assembly Design", Nuclear Engineering and Design, Vol. 237, 2007, pp.716-731.
- [7] In, W. K. and Chun, T. H., "CFD Analysis of a Nuclear Fuel Bundle Test for Void Distribution Benchmark", 13th International Topical Meeting on Nuclear Reactor Thermal Hydraulics(NURETH-13), Kanazawa City, Japan, 2009, Sept. 27-Oct. 2.
- [8] ANSYS Inc., ANSYS CFX-Solver, Release 12.1, 2009.
- [9] Ishii, M. and Mishima, K., "Two-Fluid Modeling and Hydrodynamic Constitutive Relations," Nuclear Engineering and Design, Vol. 82, 1984, pp. 107-126.
- [10] Ishii, M. and Zuber, M., "Drag Coefficient and Relative Velocity in Bubbly, Droplet or Particulate Flows", *AIChE J.*, Vol. 25, 1979, pp. 843-855.
- [11] Zun, I., "The Transverse Migration of Bubbles Influenced by Walls in Vertical Bubbly Flow," *Int. J. Multiphase Flow*, Vol. 6(6), 1980, pp.583-588.
- [12] Tomiyama, A., Tamai, H. T., Zun, I. and Hosokawa, S., "Transverse Migration of Single Bubbles in Simple Shear Flows," Chemical *Engineering and Science*, Vol. 57, 2002, pp.1849-1858.
- [13] Hibiki, T. and Ishii, M., "Lift Force in Bubbly Flow Systems," Chemical *Engineering* and Science, Vol. 62, 2007, pp.6457-6474.
- [14] Antal, S. P., Lahey Jr., R.T. and Flaherty, J.E., "Analysis of Phase Distribution in Fully Developed Laminar Bubbly Two-Phase Flow," *Int. J. Multiphase Flow*, Vol. 17(5), 1991, pp.635-652.
- [15] Burns, A. D, Frank, T., Hamill I. and Shi, J., The Favre Averaged Drag Model for Turbulent Dispersion in Eulerian Multi-Phase Flows, *ICMF'2004*, 5th International Conference on Multiphase Flow, 2004, Yokohama, Japan.
- [16] Sato, Y., Sadatomi, M. and Sekoguchi, K., "Momentum and Heat Transfer in Two-Phase Bubbly Flow I," *Int. J. Multiphase Flow*, Vol. 7, 1981, pp.167-177.
- [17] Mikic, B. B. and Rohsenow, W. M., "A New Correlation of Pool-Boiling Data including the Fact of Heating Surface Characteristics," *ASME J. Heat Transfer*, Vol. 91, 1969, pp.245-250.
- [18] Rubin, A., Schoedel, A., Avramova, M, Utsuno, H., Bajorek, S. and Velazquez-Lozada, A., OECD/NRC Benchmark Based on NUPEC PWR Subchannel and Bundle Tests (PSBT) Vol. I: Experimental Database and Final Problem Specification, 2010, NEA/NSC/Doc(2010).